J Mater Sci (2019) 54:14218–14232

Polymers & biopolymers

Dual ionically cross-linked hydrogels with ultra-tough, stable, and self-healing properties

Bo Xu[1], Xiong Zhang[1], Shuchun Gan[1], Jianhao Zhao[1], and Jianhua Rong[1,*]

[1] *Department of Materials Science and Engineering, College of Chemistry and Materials Science, Jinan University, Guangzhou 510632, China*

Received: 26 February 2019
Accepted: 12 June 2019
Published online: 8 August 2019

ABSTRACT

Excellent mechanical and self-healing features could make hydrogels an ideal candidate for the application of load-bearing soft tissue replacements such as cartilage. In this study, a dual ionically cross-linked 2-hydroxypropyltrimethyl ammonium chloride chitosan (HACC)/poly(acrylic acid) (PAAc)-Fe^{3+} hydrogel was constructed using a one-pot method (in situ polymerization of AAc in the presence of HACC and Fe^{3+}). Both macromolecular positively charged HACC and Fe^{3+} metal ions acted as cross-linkers to form ionic bonds with negatively charged PAAc. The HACC/PAAc-Fe^{3+} hydrogels demonstrated ultra-high mechanical strengths (tensile strength of ca. 9.86 MPa and compressive stresses greater than 95 MPa at 99% strain), excellent self-recoverability (ca. over 90% toughness recovery within 5 h without any external stimuli), outstanding self-healing properties (ca. 74% self-healing efficiency at 70 °C for 48 h), transparency, and high stabilities in aqueous environments. The mechanical properties of the hydrogels could be adjusted by varying the concentration of HACC and Fe^{3+}. This work provides a new approach for the construction of novel tough and transparent hydrogels with a fully ionically cross-linked network.

Abbreviations

3T3	Mouse embryo fibroblasts
AAc	Acroleic acid
APS	Ammonium persulfate
ATR-FTIR	Attenuated total reflectance Fourier-transform infrared
CCK-8	Cell counting kit-8
DMEM	Dulbecco's modified eagle's medium
FBS	Fetal bovine serum
HACC	2-Hydroxypropyltrimethyl ammonium chloride chitosan
PAAc	Polyacrylic acid
PAM	Polyacrylamide
SEM	Scanning electron microscope
UV–Vis	Ultraviolet–visible
XG	Xanthan gum

Address correspondence to E-mail: trong@jnu.edu.cn

https://doi.org/10.1007/s10853-019-03773-5

Introduction

Hydrogels, which are soft-wet materials that consist of a large amount of water and a three-dimensional cross-linked polymer network [1], have been widely used in biomedical applications such as biomaterials for wound healing, drug delivery, substitutes, and the repair of soft tissues, tissue engineering, and biosensors [2–8]. In recent years, significant effort was directed toward the improvement in the mechanical properties of hydrogels, to meet the application requirements for soft tissue replacements such as cartilages, tendons, and ligaments; in addition to double network (DN) gels [9–12], nanocomposite gels [13, 14], tetra-PEG gels [15], macromolecular microparticle composite gels [16, 17], hydrogen bonding gels [18], hydrophobic association gels [17, 19], and polyampholyte or polyion gels [20–22]. Self-healing features make hydrogel an ideal candidate for the construction of biomedical materials. The remarkable performances of hydrogels are typically demonstrated by physical cross-linking (non-covalent bonding) between polymer chains. Recently, non-covalent cross-linking routes were developed, which include hydrogen bonding [18, 23, 24], metal coordination interactions [9, 25, 26], ionic bonds [21, 22], hydrophobic interactions [12, 19], host–guest interactions [27], π–π stacking [28, 29], and chain entanglement [30, 31]; or a combination of the above-mentioned interactions. Wang et al. [26] developed a dual physically cross-linked hydrogel that was triggered by clay nanosheets and iron ions (Fe^{3+}) as cross-linkers. The hydrogel achieved a high stretchability, toughness, and recoverability; however, it lacked the self-healing characteristic when destroyed. Ren et al. [32] designed polyelectrolyte hydrogels that consist of natural polysaccharides and their derivatives (alginate and 2-hydroxypropyltrimethyl ammonium chloride chitosan), which formed reversible polyelectrolyte complexes with opposite charges. The hydrogels demonstrated excellent self-healing performances. The self-healing was achieved in 7 h without any external intervention, which resulted in a poor mechanical property.

As previously reported, dual physically cross-linked polyacrylamide/xanthan gum (PAM/XG) DN hydrogels were synthesized by the formation of metal coordination interactions and hydrophobic interactions [12]. The PAM/XG DN hydrogels exhibited fracture stresses as high as 3.64 MPa and compressive stresses at 99% strain that were greater than 50 MPa. In addition, the PAM/XG DN hydrogels demonstrated an excellent fatigue resistance, notch-insensitivity, and remarkable self-healing properties, which may result from their distinctive physical cross-linking structures. However, the PAM/XG hydrogels lost their self-healing properties after water swelling measurements due to the destruction of hydrophobically associated cross-linking structures during swelling. Zhao et al. [33] also produced a dual dynamic cross-linked poly(-vinyl alcohol)/4-carboxyphenylboronic acid/calcium hydrogel that contained borate bonding and ionic interactions to bridge the polymer chains, which exhibited an ultra-high strength and self-healing capability. However, the hydrogel did not exhibit good self-recoverability. Nevertheless, it is a challenge to realize excellent mechanical properties, outstanding fatigue resistance, and self-healable hydrogels.

In this study, a dual ionically cross-linked strategy was developed to manufacture tough, transparent, and self–healing hydrogels with excellent fatigue resistances. In particular, the hydrogels were synthesized by the in situ polymerization of acrylic acid in a mixed solution of 2-hydroxypropyltrimethyl ammonium chloride chitosan (HACC) and iron ions (Fe^{3+}), in which the ionic bonds between positively charged HACC and oppositely charged PAAc acted as the first set of cross-linking points, and the ionic interaction between trivalent iron ions and carboxyl groups was used as the second set of ionic cross-linking points. Dual dynamic reversible physical cross-linked points result in hydrogels with excellent mechanical properties, excellent self-recovery, and self-healing capabilities.

Experimental section

Materials

The 2-hydroxypropyltrimethyl ammonium chloride chitosan (HACC, the degree of substitution > 90%, Mw: 2×10^5) was purchased from Guangdong Weng Jiang Chemical Reagent Co., Ltd. Acrylic acid (AAc) and sodium chloride (NaCl) were obtained from

Aladdin (Shanghai, China) Inc. In addition, the $FeCl_3{\cdot}6H_2O$ was purchased from the Damao Chemical Regent Factory (Tianjin, China), and ammonium persulfate (APS) was purchased from the Fuchen Chemical Regent Factory (Tianjin, China). The cell counting kit-8 (CCK-8) was purchased from the Beyotime Institute of Biotechnology (Shanghai, China). Moreover, Dulbecco's modified Eagle's medium (DMEM) and fetal bovine serum (FBS) were purchased from the Invitrogen Corporation (Washington, USA). All the chemicals were used as received.

Synthesis of HACC/PAAc hydrogels and HACC/PAAc-Fe^{3+} hydrogels

The HACC/PAAc-Fe^{3+} hydrogels were fabricated using a one-pot method. The HACC (2.32 g) was first dissolved in 11.6 mL of deionized water to form the HACC aqueous solution under vigorous stirring for 2 h at room temperature. Thereafter, AAc (2.55 mL, density of 1.06 g mL^{-1}) and $FeCl_3{\cdot}6H_2O$ (1.0%, 1.4%, 2.0%, 3.3%, or 5.0%, molar ratio of $FeCl_3{\cdot}6H_2O$/AAc) were added into the HACC solution while stirring for 1 h at room temperature. After the addition of APS (0.054 g, 2 wt% of AAc monomer), the mixed solution was rapidly de-gassed and then injected into two glass slides with a spacer of 2 mm and plastic molds (diameter: 10 mm, and height: 8 ± 1 mm). Finally, the reaction was maintained at 70 °C for 24 h for the formation of HACC/PAAc-Fe^{3+} hydrogels. The as-prepared hydrogels were dialyzed in deionized water for at least 7 days with changing water every 12 h, to remove residue and adjust the cross-linked hydrogel network. The HACC/PAAc hydrogels were prepared using the same process; however, $FeCl_3{\cdot}6H_2O$ was not added. The dialyzed (or equilibrated) hydrogels were denoted as HACC-*n*/PAAc and HACC-*n*/PAAc-Fe^{3+}-*m*, where *n* stands for the mass/volume ratio of HACC to deionized water (*n* = 0.10 g mL^{-1}, 0.125 g mL^{-1}, 0.15 g mL^{-1}, 0.175 g mL^{-1}, 0.20 g mL^{-1}, and 0.25 g mL^{-1}) and *m* stands for the molar ratio of $FeCl_3{\cdot}6H_2O$ relative to AAc (*m* = 1.0%, 1.4%, 2.0%, 3.3% and 5.0%).

Mechanical test

The mechanical property tests were carried out on the as-prepared and equilibrated hydrogels using a universal testing machine (Zwick/Roell Z005, Germany) at room temperature. For the tensile tests, the hydrogel samples with thicknesses of 2.0 mm were sliced into rectangles (length: 30 mm, and width: 4 mm). The speed of the tensile and loading–unloading tests was fixed at 100 mm min^{-1} [21]. For the cyclic tensile measurements, the gels were immersed in water prior to the next loading–unloading test, to prevent the loss of water. The stress σ was estimated from the load divided by the cross-sectional area of the undeformed sample. The strain ε was estimated from the clamp displacement divided by L_0 (the initial distance between the two clamps of the tester) [20]. The Young's modulus E was calculated from the slope of the linear regions of the stress–strain curves at small strain (within 10%). The work of extension at fracture (toughness of hydrogel) W_b was calculated from the integral area of the tensile stress–strain curve until fracture. For the compression tests, cylindrical hydrogel samples (diameter: ~ 5 to 8 mm, and height: ~ 4 to 6 mm) were tested at a constant velocity of 2 mm min^{-1} in compression. Moreover, the loading speed was 10 mm min^{-1} in cyclic compression tests to reduce the loss of water. For each sample, a minimum of three measurements were carried out, and averages were obtained.

Fourier-transform infrared and ultraviolet–visible spectroscopy analyses

The Fourier-transform infrared (FTIR) spectra of the pure PAAc, pure HACC, PAAc-Fe^{3+}, HAAC/PAAc, and HACC/PAAc-Fe^{3+} hydrogels were analyzed to determine possible cross-links between HACC and PAAc. The samples were dialyzed in deionized water to eliminate residues from the samples. The FTIR spectra of these freeze-dried samples were recorded between 4000 and 500 cm^{-1} using attenuated total reflectance FTIR (ATR-FTIR, Bruker VERTEX70, Germany). The UV–Vis spectra of the sliced hydrogels were recorded using ultraviolet–visible spectroscopy (UV-2550, Shimadzu, Japan).

SEM morphology of the hydrogels

The structures of the hydrogels were examined using an Ultra55 field emission scanning electron microscope (SEM; Zeiss, Germany). The sample gels were frozen at − 20 °C and then freeze-dried for 24 h. The obtained freeze-dried gels were cut to expose their inner structures. Prior to the SEM examination, the

surfaces were coated with a thin layer of gold using the sputtering method.

Self-healing experiment

The HACC-0.20/PAAc and HACC-0.20/PAAC-Fe^{3+}-2.0 hydrogels were tested using self-healing experiments. To evaluate the self-healing properties of the gel samples, the specimens were first cut into two segments; the cross sections of which were coated with deionized water or NaCl solution, and then fixed in contact to heal for a certain time-period in a water bath at a given temperature for self-healing. The tensile testing speed of the healed samples was set as 100 mm min^{-1}.

Swelling behavior

The as-prepared and equilibrium water contents of the HACC/PAAc and HACC/PAAc-Fe^{3+} hydrogels were measured using a gravimetric method at room temperature, as follows. The cylindrical as-prepared hydrogel samples were fully immersed in the deionized water. The swollen samples were weighed at specific time intervals until they reached swelling equilibrium. Thereafter, the hydrogels were dried in a vacuum oven at 60 °C for 48 h, and a constant weight was obtained. The as-prepared and equilibrium water contents of the hydrogels were calculated using the following equations:

$$\text{As-prepared water content} = \frac{w_o - w_{dry}}{w_o} \times 100\% \quad (1)$$

$$\text{Equilibrium water content} = \frac{w_{sw} - w_{dry}}{w_{sw}} \times 100\% \quad (2)$$

where w_o is the original weight, w_{sw} is the swollen weight of the as-prepared hydrogel, and w_{dry} is the dry weight of the cylindrical hydrogel.

In vitro cytotoxicity

The cytotoxicity was evaluated using the CCK-8 method. The HACC/PAAc and HACC/PAAc-Fe^{3+} hydrogels were used to investigate the behaviors of 3T3 cells. The HACC/PAAc and HACC/PAAc-Fe^{3+} hydrogels were freeze-dried and fully immersed in complete DMEM (with high glucose and 10% fetal bovine serum supplemented) for 24 h at 37 °C, to achieve the swelling equilibrium, thus preventing the absorption of the culture medium during incubation with cells. The hydrogel was cut into a cylinder with a diameter of 5 mm and a thickness of 1 mm. And then the hydrogel was sterilized by irradiating under UV light for 1 h. Thereafter, 3T3 cells were cultured on a 24-well plate (10^5 cells/well) with a complete DMEM culture medium in a humidified atmosphere of 5% CO_2 at 37 °C. After culturing for 24 h, the culture medium was replaced, and the cells without hydrogels acted as a negative control group. The hydrogel and complete DMEM were removed in a perforated plate after incubation for 24 h and 48 h, respectively. Finally, the cell viability was measured using CCK-8 kits.

$$\text{Cell viability}(\%) = [A_{eg} - A_b]/[A_{ncp} - A_b] \times 100\%$$

where A_{eg} is the absorbance of the wells with respect to the cells, CCK-8 solution, and extracted fluid of hydrogels; A_{ncp} is absorbance of the wells with respect to the cells and CCK-8 solution; and A_b is the absorbance of the wells with respect to the medium and CCK-8 solution without cells.

Furthermore, the HACC/PAAc and HACC/PAAc-Fe^{3+} hydrogels were soaked in complete DMEM (with high glucose and 10% fetal bovine serum supplemented) for 24 h at 37 °C to reach the swelling equilibrium, thus preventing the absorption of the culture medium during incubation with the cells. The hydrogel was cut into a cylinder with a diameter of 5 mm and a thickness of 1 mm. Moreover, 3T3 cells were seeded on a hydrogel surface and co-cultured into a 96-well plate for 24 h, and then 200 μL glutaraldehyde was added into each well overnight. After the removal of residual glutaraldehyde with PBS, the cells were step-by-step dehydrated using ethanol/water solutions (70%, 80%, 90%, 100% and 100%, respectively) for 10 min at each step. The morphologies of the 3T3 cells on the gel, coated with a thin layer of gold, were investigated using an SEM (Zeiss, Germany).

Results and discussion

Synthesis of hydrogels

The dual ionically cross-linked hydrogels (i.e., HACC/PAAc-Fe^{3+} hydrogels) were synthesized using a "one-pot" method, as illustrated in Fig. 1. The AAc monomer, Fe^{3+}, and an initiator (APS) were first added to the HACC solution, in which the in situ polymerization of AAc was initiated to form

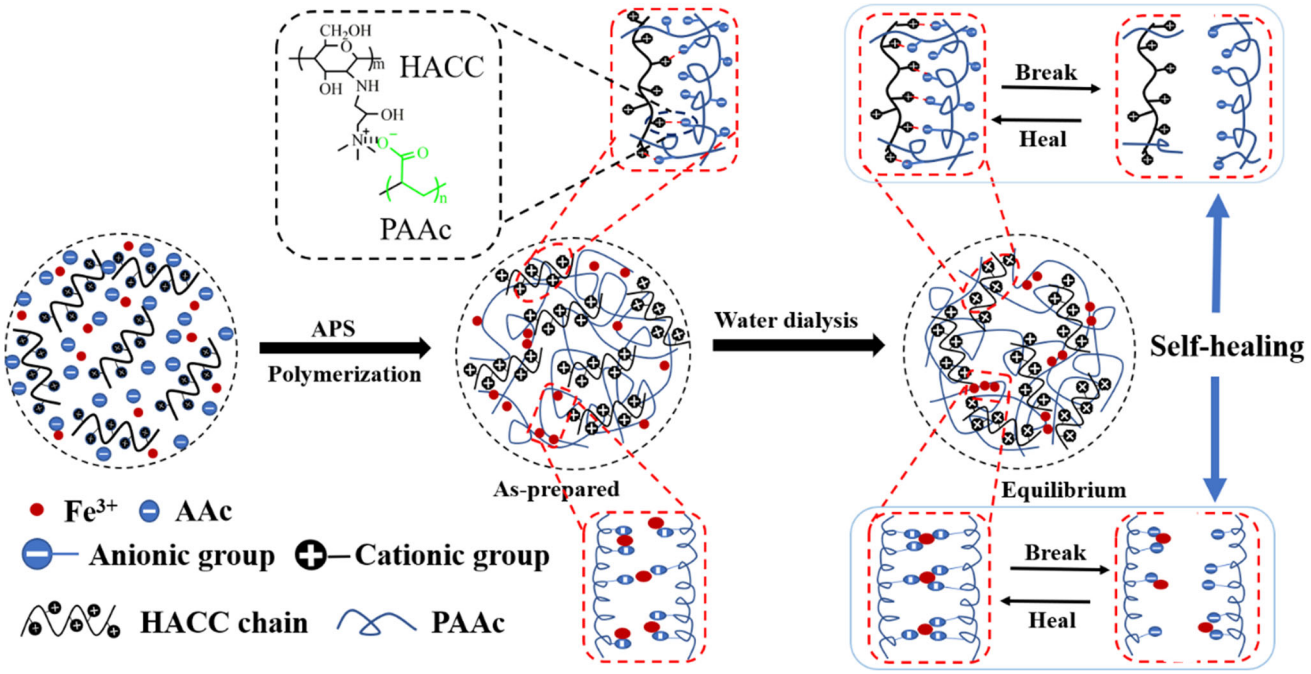

Figure 1 Schematic diagram of the preparation of the HACC/PAAc-Fe^{3+} hydrogel and a possible network structure of the HACC/PAAAc-Fe^{3+} hydrogel.

hydrogels. The as-prepared hydrogels were then dialyzed in deionized water for at least 7 days, during which the water was changed every 12 h, to form the equilibrium state hydrogels. For the single ionically cross-linked HACC/PAAc hydrogel, all the steps were same, with the exception of the first step without Fe^{3+}. The detailed synthesis procedures are presented in "Synthesis of HACC/PAAc hydrogels and HACC/PAAc-Fe^{3+} hydrogels" section. In the dual ionically cross-linked hydrogels, positively charged HACC and Fe^{3+} acted as macromolecular and small molecular cross-linkers, respectively, for the formation of ionic bonds with the carboxyl groups of PAAc. During the polymerization of AAc, only a portion of the ionic bonds were formed because the pH value of the solution was less than 2. Hence, the ionization of PAAc was suppressed, and only a few $-COO^-$ groups were present in the solution. An increasing number of bonds were formed as the dialysis proceeded with higher pH values, until they reached the equilibrium states. However, the contributions of the HACC and Fe^{3+} cross-linking bonds to the hydrogels were considered as significantly different.

Mechanical properties

The tensile and compressive stress–strain curves of the HACC/PAAc hydrogels are presented in Fig. 2. Significant differences were observed between the mechanical properties of the as-prepared and equilibrated samples. The typical tensile stress–strain curves of the as-prepared and equilibrated HACC/PAAc hydrogels are presented in Fig. 2a, b, respectively. The as-prepared HACC/PAAc hydrogels were soft and flexible. The elongation at break of the hydrogel of HACC-0.1/PAAc was 2800%; however, its fracture stress was 0.113 MPa. After dialysis, the tensile properties of all the HACC/PAAc hydrogels increased significantly. For example, the tensile strength, elastic modulus, and toughness of the equilibrated HACC-0.15/PAAc hydrogel reached 3.81 MPa, 0.81 MPa, and 15.48 MJ m^{-3}, respectively; which were higher than the values of the corresponding as-prepared hydrogels by factors of 19.1, 15.3, and 7.7, respectively. However, the elongation at break was decreased from 2126 to 1281%. With a gradual increase in the HACC concentration from 0.10 to 0.15 g mL^{-1}, the hydrogel strength increased monotonously with a decrease in the corresponding elongation at break. As observed, the more compact network in the equilibrated hydrogels was formed

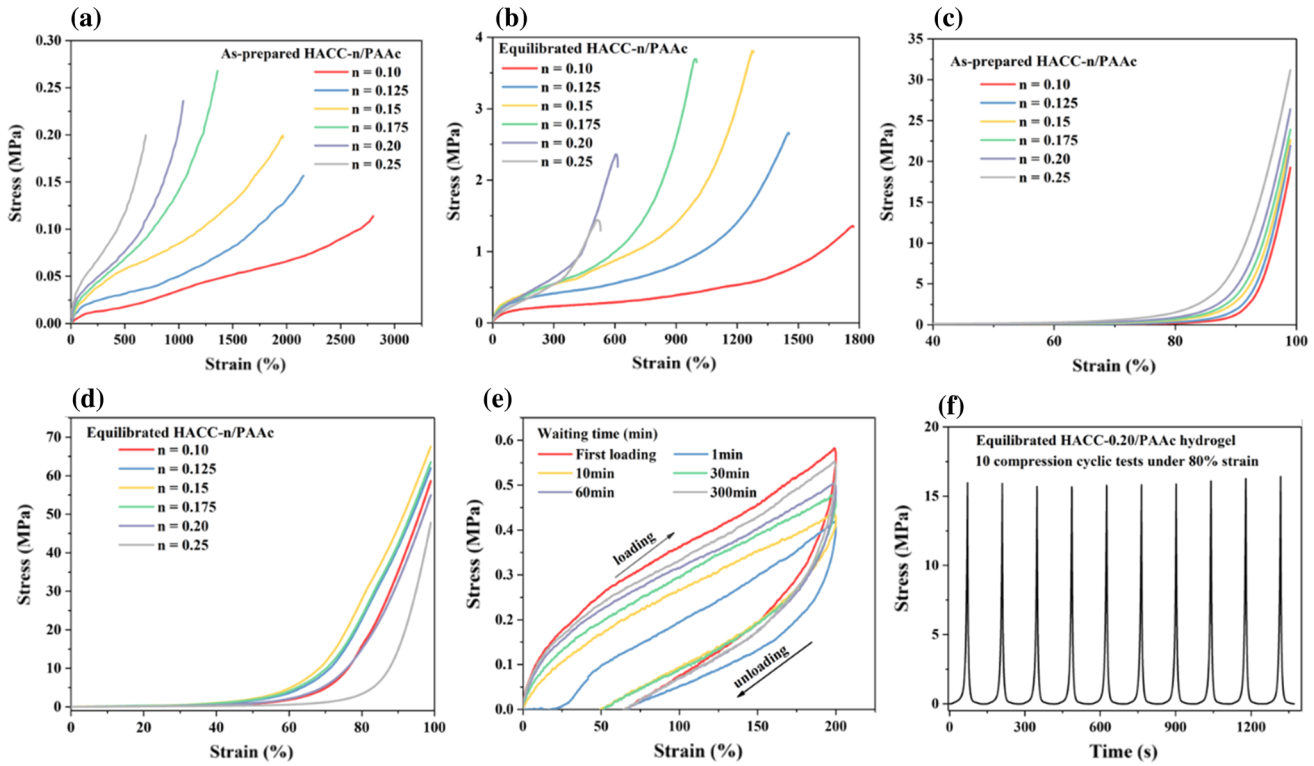

Figure 2 Tensile stress–strain curves of HACC/PAAc hydrogels at **a** as-prepared and **b** equilibrated states; compressive stress–strain curves of HACC/PAAc hydrogels at **c** as-prepared and **d** equilibrated states; **e** recovery curves of HACC-0.2/PAAc hydrogel under 200% strain and **f** cyclic stress-time compression tests of the HACC-0.2/PAAc hydrogel under 80% strain.

due to the increased ionic bonds between $-R_3N^+$ of HACC and $-COO^-$ of PAAc in the dialysis process, which significantly enhanced the mechanical strength of the hydrogels. The detailed performance data are summarized in Table S1.

However, the tensile strength, elastic modulus, and toughness of the equilibrated HACC/PAAc hydrogels decreased when the HACC concentration was increased from 0.175 to 0.25 g mL^{-1} (see Fig. 2b). The compression test results of the as-prepared and equilibrated HACC/PAAc hydrogels (see Fig. 2c, d) revealed that all the gel samples could be compressed to 99% without fracture. Significant differences were observed in the compression behaviors of the as-prepared and equilibrated PAAc/HACC hydrogels, as in the tensile test. The HACC-0.15/PAAc hydrogel exhibited an excellent stress performance (65 MPa) at 99% compression strain. The higher HACC concentration also exerted adverse effects on the compressive strengths and moduli of the equilibrated HACC/PAAc hydrogels, similar to the tensile performance, as shown in Fig. 2d.

The equilibrated HACC/PAAc hydrogels also demonstrated excellent recovery properties. The HACC-0.20/PAAc hydrogel was selected for the tensile loading–unloading tests at a strain of 200% without any external stimuli. As shown in Fig. 2e, after the first loading–unloading cycle under 200% strain, a 27% residual strain was observed. However, the residual strain gradually decreased with the resting time, and then disappeared after 10 min. With an increase in the resting time, the second test curve shifted closer to the first test curve. The hysteresis ratio (i.e., the ratio between the hysteresis areas that correspond to the second and first cycles) reached 94.2% after 300 min, which indicated that the HACC-0.2/PAAc hydrogel network structure was nearly completely restored. As illustrated in Fig. 2f of the repeated compression test, the equilibrated HACC-0.20/PAAc hydrogel maintained its compression stress at a compression strain of 80% after 10 loading–unloading cycles, thus demonstrating its good fatigue resistance.

The HACC/PAAc-Fe^{3+} hydrogels were prepared using different concentrations of Fe^{3+} with a constant

HACC concentration of 0.20 g mL^{-1}. Figure 3 presents the tensile and compressive tests results of the hydrogels with different Fe^{3+} concentrations. Compared with the as-prepared HACC/PAAc hydrogel (m = 0, in Fig. 3a), the stress and strain of the as-prepared HACC/PAAc-Fe^{3+} gel decreased, whereas the tensile properties of all the equilibrated HACC/PAAc-Fe^{3+} hydrogels increased significantly (Fig. 3b); which is similar to HACC/PAAc hydrogels. With an increase in the Fe^{3+}/AAc molar ratio from 1.0 to 5.0%, the elastic modulus of all the hydrogels gradually increased. However, the elongation at break decreased, which indicates that more rigid networks were formed with the addition of Fe^{3+}. In addition, the tensile strengths and toughness of the gels did not increase monotonously as the concentration of Fe^{3+} increased. There was a significant increase in the tensile strengths and toughness when the Fe^{3+}/AAc molar ratio increased from 1.0 to 2.0%, and a decrease with higher Fe^{3+}/AAc molar ratios (i.e., 3.3% and 5.0%). This indicates that the excessively dense cross-linked networks made the hydrogels rigid, and they were easily fractured at the relatively low strains. Hence, only a suitable Fe^{3+}/AAc molar ratio (2.0%) enabled an appropriate cross-linking density, which helped to obtain super-tough HACC-PAAc-Fe^{3+} hydrogels. When the HACC concentrations were maintained at 0.1 g mL^{-1} and 0.15 g mL^{-1} instead of 0.2 g mL^{-1}, similar results were obtained (see Fig. S3 and Table S2).

The compressive stress–strain curves of the as-prepared HACC/PAAc-Fe^{3+} hydrogels are presented in Fig. S2. The fracture strain decreased with an increase in the Fe^{3+} concentration, which indicates that the as-prepared HACC/PAAc-Fe^{3+} hydrogels were more brittle when compared with the as-prepared HACC/PAAc hydrogels. This can be attributed to the increase in the extent of cross-linking and the instability and inhomogeneity of the two physical cross-links in the hydrogels after the introduction of Fe^{3+}. After dialysis, the HACC/PAAc-Fe^{3+} hydrogels exhibited excellent compression properties, and the compression stress of the HACC-0.20/PAAc-Fe^{3+}-2.0 hydrogel was greater than 96 MPa at a

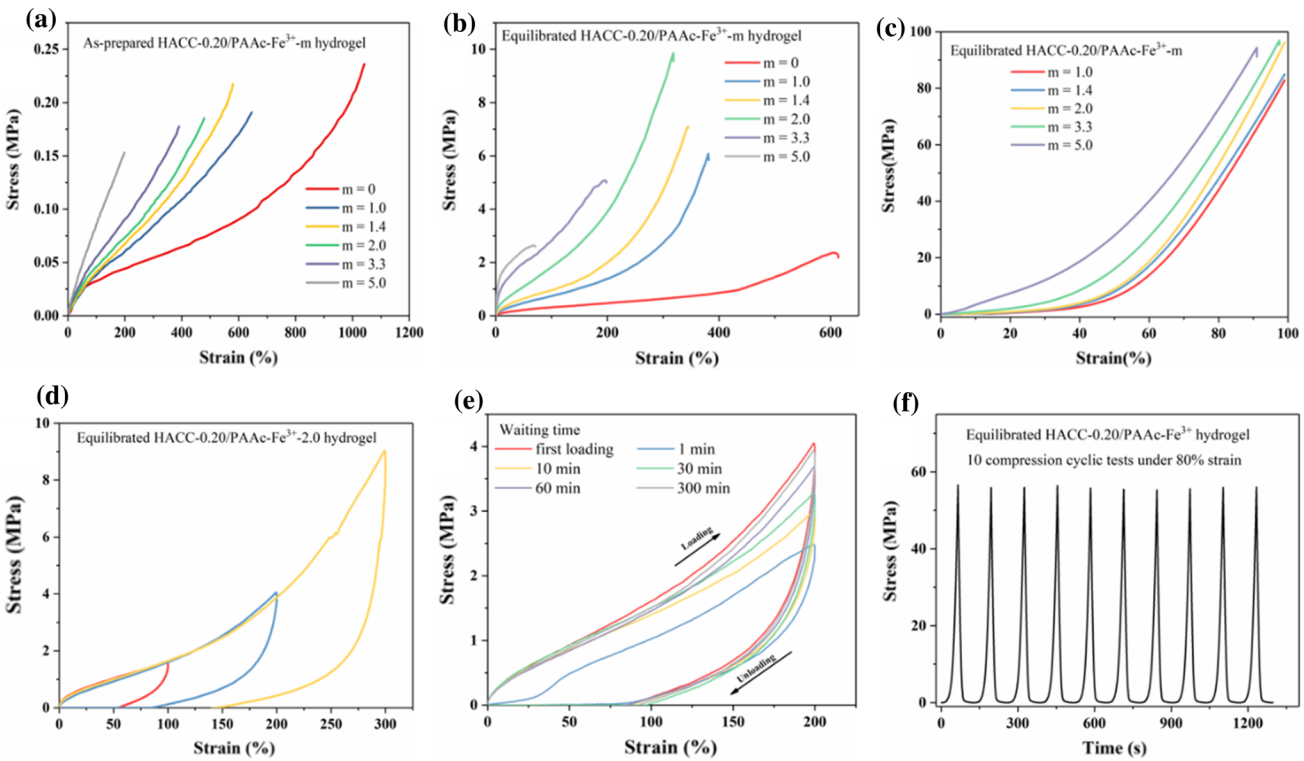

Figure 3 Tensile stress–strain curves of HACC-0.20/PAAc-Fe^{3+} hydrogels at **a** as-prepared and **b** equilibrated states; **c** compressive stress–strain curves of PAAc/HACC hydrogels at equilibrated states; **d** loading–unloading tests of HACC-0.20/PAAc-Fe^{3+}-2.0 under different strains (100%, 200% and 300%); **e** recovery curves of equilibrated HACC-0.20/PAAc-Fe^{3+}-2.0 hydrogel with different waiting times under 200% strain; **f** cyclic stress-time compression tests of HACC-0.20/PAAc-Fe^{3+}-2.0 hydrogel for 10 cycles under 80% strain.

compression strain of 99% (see Fig. 3c.). Figure 3d presents the loading–unloading curves of the HACC-0.20/PAAc-Fe^{3+}-2.0 hydrogel under varying strains. All the loading–unloading curves of the HACC-0.20/PAAc-Fe^{3+}-2.0 hydrogel exhibited clear hysteretic loops, which indicates that the hydrogels could dissipate energy effectively. Further loading–unloading tests were conducted at a strain of 200% to evaluate the self-recoverability of the HACC-0.20/PAAc-Fe^{3+}-2.0 hydrogel at room temperature without any external stimuli (see Fig. 3e). The residual strain was almost fully recovered after 10 min, and the hysteresis ratio reached 56.2%, which indicates that the shape of the HACC-0.20/PAAc-Fe^{3+}-2.0 could be rapidly recovered. With an increase in the resting time, the second tensile curve gradually approached the first tensile curve. The hysteresis ratios were 99.2% after 300 min later, which demonstrates the excellent self-recoverability of the HACC-0.20/PAAc-Fe^{3+}-2.0 hydrogel. Compared with the HACC/PAAc hydrogels, the HACC/PAAc-Fe^{3+} hydrogels exhibited a better recovery performance after the introduction of Fe^{3+}, which may be because the double reversible physical cross-linking points could be quickly reformed after the destruction of the hydrogel. In addition, the repeated compression tests on the HACC-0.20/PAAc-Fe^{3+}-2.0 hydrogel for 10 consecutive cyclic compression tests under 80% strain (Fig. 3f) revealed that the compression process did not cause unrecoverable damage and that the initial value of the final stress was unchanged. This confirms the excellent fatigue resistance of the hydrogel.

The results of the above analyses reveal that the mechanical properties of the hydrogels were significantly improved after the introduction of a small number of ferric ions. It was considered that Fe^{3+} played a more important role in increasing the rigidity of the hydrogels, whereas HACC played a more important role in enhancing the flexibility of the hydrogels. During the tensile process, the rigid network that formed between the carboxyl groups and Fe^{3+} was broken first, which could suitably dissipate energy. Hence, dual reversible physical cross-linking leads to tough hydrogels with excellent self-recovery and fatigue resistance characteristics.

Self-healing performance

Due to their reversible ionic bonding, the HACC/PAAc and HACC/PAAc-Fe^{3+} hydrogels were expected to possess self-healing properties. As shown in Fig. 4a, two pieces of HACC-0.20/PAAc-Fe^{3+}-2.0 hydrogel samples (one of which was dyed with methyl blue) were cut into two halves, of which the fresh surfaces were coated with a 3 M NaCl solution and then set in contact and healed at 70 °C for 48 h. The healed sample could be stretched by hand to a length greater than its original length by a factor of 3 without breaking, at which it could lift the weight of 1.72 kg. In addition, the self-healing efficiency of the hydrogel was measured under different conditions such as various coating solutions, healing times, and healing temperatures.

The self-healing efficiency of the HACC-0.20/PAAc-Fe^{3+}-2.0 hydrogel was assessed using tensile tests by comparing the fracture stress of the hydrogels before and after self-healing, i.e., w_b (self-healed)/w_b (original), where w_b is calculated from the integral area of the tensile stress–strain curve. The influences of the coating solution, healing temperature, and healing time were explored (Fig. 4). Figure 4b presents the tensile results of the healed HACC-0.20/PAAc-Fe^{3+}-2.0 hydrogels by coating the fresh fracture surfaces with different solutions. When the coating solution was deionized water, 0.154 M or 3 M NaCl solution, the self-healing efficiencies of the hydrogels were 45.4%, 53.6%, and 74.5%, respectively, which demonstrates that salt solution could promote the healing process. However, when coating the fracture surfaces with NaCl solution, the Young's modulus of the self-healed hydrogel decreased slightly when compared with that of the original sample and water coated sample, which indicates that the cross-linking density was slightly damaged, given that Na^+ replaced a small amount of Fe^{3+}. The self-healing efficiencies of the HACC-0.20/PAAc hydrogel under the same conditions were compared (Fig. 4c), which revealed that the highest healing efficiency was only 54.0% when using 3 M of NaCl as a coating solution. Figure 4d presents the influence of the healing temperature on the self-healing efficiency of the hydrogel. The hydrogel could be self-healed at lower temperatures such as 37 °C; however, the self-healing efficiency increased with an increase in the temperature, which can be attributed to the enhanced mobility of the chains at higher temperatures. Figure 4e presents the influences of the healing time on the self-healing efficiency of the HACC-0.20/PAAc-Fe^{3+}-2.0 hydrogel using deionized water as a coating solution. The Young's modulus of the self-healed

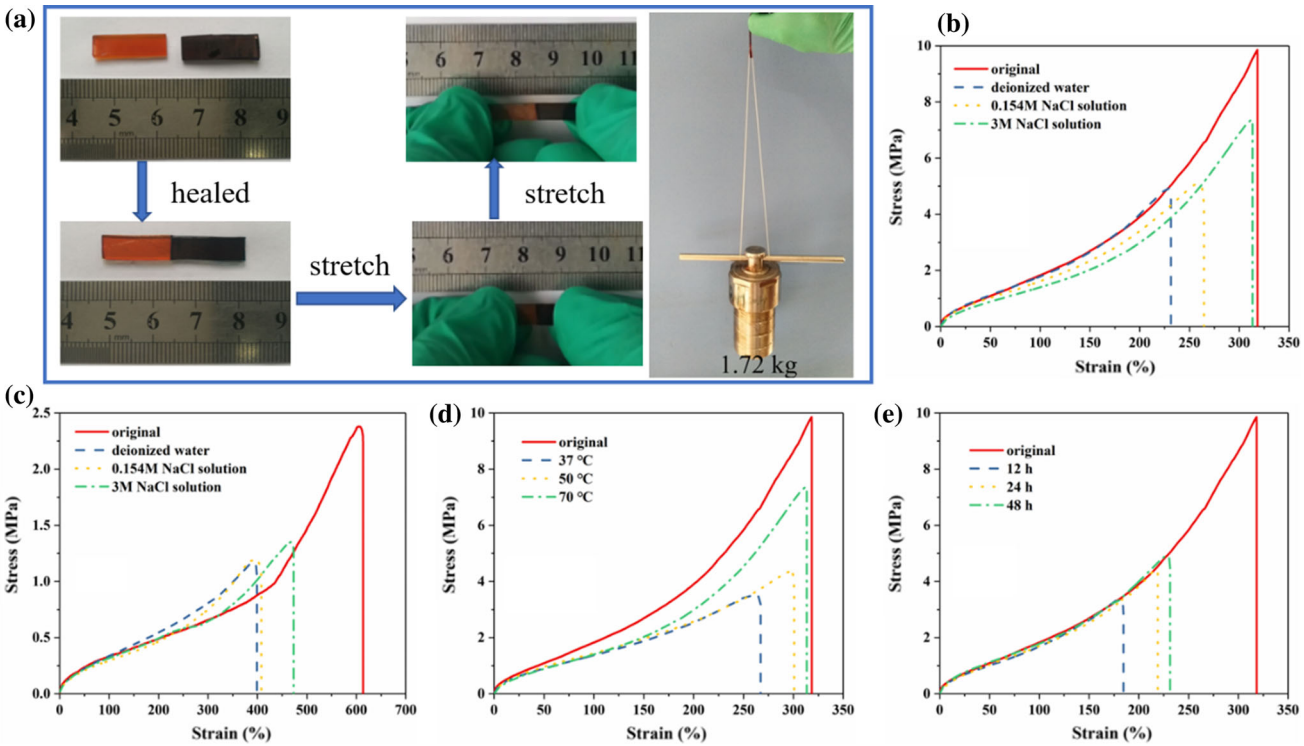

Figure 4 **a** Images depicting self-healing behavior of HACC-0.20/PAAc-Fe^{3+}-2.0 hydrogel; **b** healing efficiencies of the HACC-0.20/PAAc-Fe^{3+}-2.0 hydrogel healed using different coating solutions at 70 °C for 48 h; **c** healing efficiencies of the HACC-0.20/PAAc hydrogel with different coating solutions at 70 °C for 48 h; **d** healing efficiencies of the HACC-0.20/PAAc-Fe^{3+}-2.0 hydrogel healed at different temperatures for 48 h and using 3 M NaCl as coating solution; and **e** healing efficiencies of the HACC-0.20/PAAc-Fe^{3+}-2.0 hydrogel healed for different healing times at 70 °C and using deionized water as coating solution.

hydrogels almost exactly coincided with that of the original hydrogel, which indicates that the cross-linking density of all the hydrogels was restored to its original value after self-healing. The self-healing efficiencies of the hydrogels with healing times of 1 h, 24 h, and 48 h were estimated as 30.0%, 38.2%, and 45.4%, respectively, which demonstrates that a longer time-period is conducive to better self-healing.

The data presented above revealed that the introduction of Fe^{3+} improved the self-healing efficiency of hydrogel, which further proved that dual physical cross-linking resulted in the excellent hydrogel properties.

The self-healing process of the dual ionically cross-linked hydrogels was conjectured, as shown in Fig. 5. When the gel was fractured, the dual reversible ionic bonds broke. The cross section was then coated with a small amount of NaCl solution and contacted together. Due to the shielding effect of the counterions, the charged polymer chains exposed to the surface were more easily diffused from one side to the other, and heating could facilitate the motion of the chains. Without the shielding effect of the NaCl counterions, highly cross-linked networks limited the mobility of the polymer chains and hindered the reconstruction of stable and dense ionic bonds in the self-healing process.

Swelling behavior

Compared with the as-prepared gels, the HACC/PAAc hydrogels and HACC/PAAc-Fe^{3+} hydrogels contracted after dialysis (Fig. 6), which indicates that the cross-linking densities of the equilibrated hydrogels were significantly higher than those of the as-prepared hydrogels. The water content of the equilibrated HACC/PAAc hydrogels decreased first, and then increased with an increase in the HACC concentration from 0.1 to 0.25 g mL^{-1}, with the lowest value of 25.6% at 0.15 g mL^{-1}, which indicated that the cross-linking density reached was highest at an HACC concentration of 0.15 g mL^{-1}. The HACC/

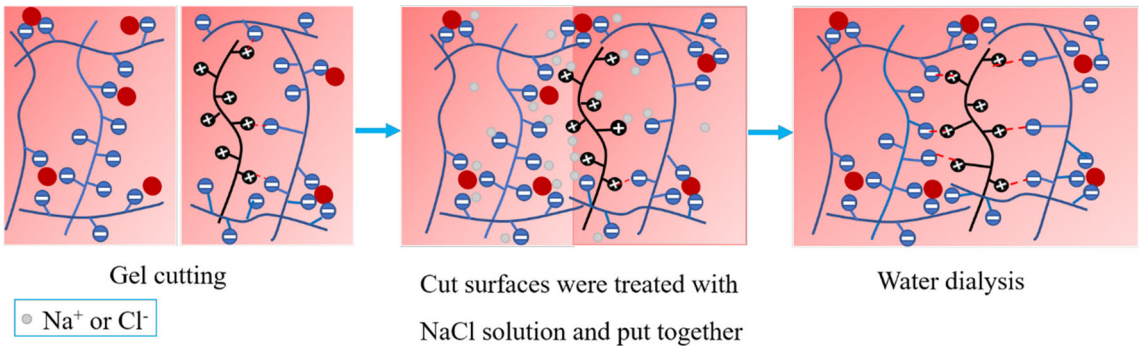

Figure 5 Schematic of the self-healing mechanism of HACC/PAAc-Fe^{3+} hydrogel.

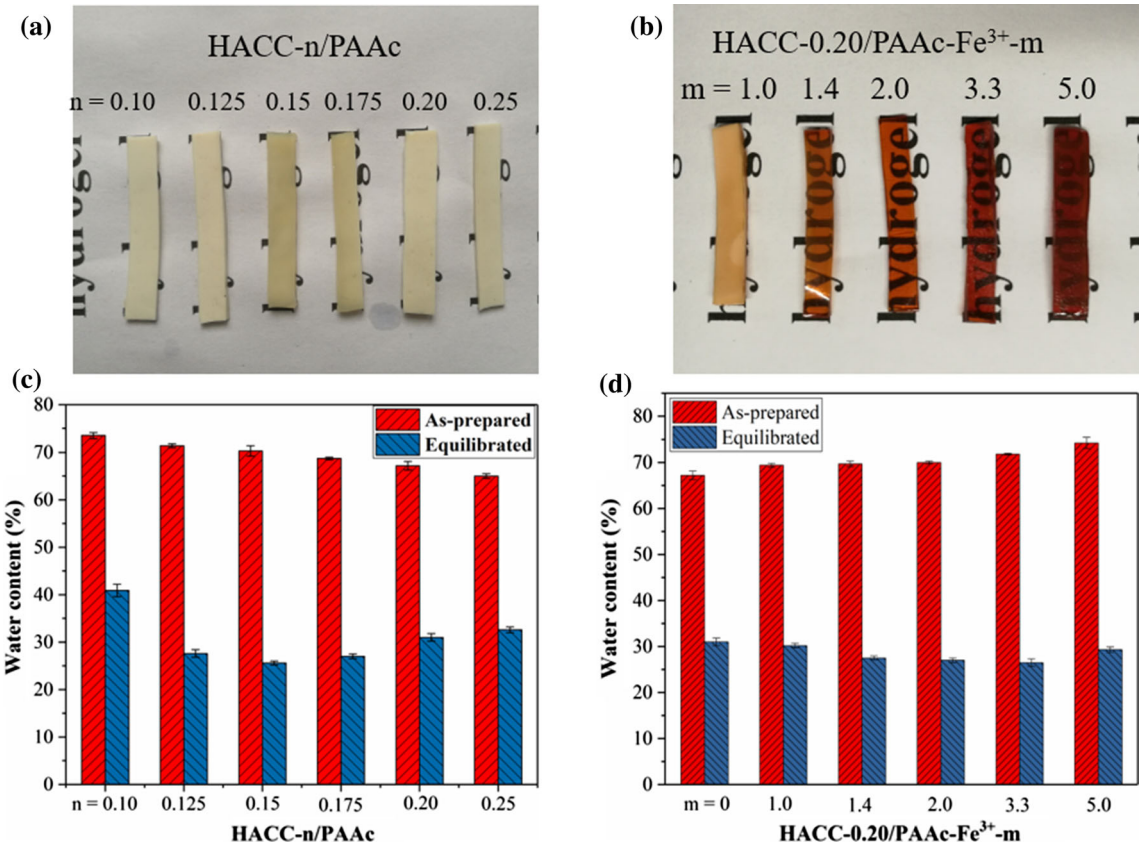

Figure 6 **a** Image of equilibrium state HACC-*n*/PAAc hydrogels **b** and HACC-0.20/PAAc-Fe^{3+}-*m* hydrogels; **c** water content of the HACC-*n*/PAAc hydrogels and **d** HACC-0.10/PAAc-Fe^{3+}-*m* hydrogels at as-prepared and equilibrated states.

PAAc hydrogels [34] were prepared under the partial shielding effect of NaCl salt ions with water contents higher than 50%, which was significantly higher than that of the hydrogels in this work. This is because the addition of NaCl salt ions affected the conformation of macromolecular chains, which could only curl in the solution of highly concentrated salt ions, thus resulting in the lower degree of cross-linking.

Compared with the HACC/PAAc hydrogel (see Fig. 6c), the water content of the as-prepared HACC/PAAc-Fe^{3+} hydrogels increased from 67.2% to 69.4–74.2%, whereas that of the equilibrated HACC/PAAc-Fe^{3+} hydrogels decreased slightly from 31.0% to 30.2–26.5%. The reason for the higher water content in the as-prepared HACC/PAAc-Fe^{3+} hydrogels may be that the weak ionic bonds in the HACC/PAAc were partially replaced by metal coordination

interactions, due to the stronger ability of Fe^{3+} to bond with carboxyl groups. However, there was a small number of $–COO^-$ groups in the solution due to the low pH value; thus, the iron ions could only form single- or double-ligands with PAAc, which did not contribute to cross-linking. Upon dialysis, an increasing number of $–COO^-$ groups were celebrated. Hence, the triple-ligand cross-link formed between Fe^{3+} and $–COO^-$, in addition to that between the quaternary ammonium groups and $–COO^-$, resulted in a higher cross-linking density and therefore lower water contents in the equilibrated HACC/PAAc-Fe^{3+} hydrogels. The water contents of the equilibrated HACC-0.20/PAAc-Fe^{3+} hydrogels ranged from 26.5 to 30.2%, which was slightly lower than that of the equilibrated HACC-0.20/PAAc. However, the mechanical properties were significantly improved. Moreover, Fig. 6a and b also reveals that the hydrogels exhibited good transparency after the introduction of iron ions. In general, the homogeneity and porosity of the materials determine the optical transmittance [35]. It was suggested that the introduction of iron ions was beneficial to form a homogeneous and compact structure of the hydrogels. It was speculated that the cross-linking degree of hydrogel increased because of the introduction of Fe^{3+}, which made the microphase size of the two polymer chains smaller than the wavelength of visible light [35]. Generally, when the microphase size is smaller than the visible wave length, the material becomes transparent. It can also be seen from the SEM images (Fig. 9c) that had a uniform and dense network structure. In addition, the pore wall of the hydrogel might become more hydrophilic because of the introduction of Fe^{3+}, which enabled more water to penetrate into the pore wall. Therefore, the refractive index difference between the pore water and pore wall was reduced and the transparency was increased.

In addition, the stability of the HACC-0.20/PAAc-Fe^{3+}-2.0 hydrogel in the NaCl solution was checked for 7 days. As shown in Fig. 7, the hydrogel exhibited good mechanical stability in the 0.154 M NaCl solution (the ionic strength of the physiological condition). However, the higher concentration of salt solution (i.e., 1 M) led to a significant decrease in the elastic modulus and fracture stress, whereas the breaking strain increased. The results indicate that the ionic cross-linking was unstable in the concentrated NaCl solution, and some ionic bonds of the hydrogels were broken in the 1 M NaCl solution because of charge shielding [21]. However, low concentration of NaCl solution (0.154 M) had little effect on the stability of hydrogel, so hydrogels were not affected in the practical application.

Structure characterization of hydrogels

The formation of an ionically cross-linked network of gels was confirmed by FTIR and UV–Vis spectra (Fig. 8). The peaks at 1478 cm^{-1}, 1590–1700 cm^{-1}, and 1400–1500 cm^{-1} are attributed to the bending vibration of $–CH_3$, and the asymmetric and symmetric stretching vibrations of carboxyl groups [36], respectively. Compared with the FTIR spectra of PAAc (Fig. 8a, curve i), HACC (curve ii), and PAAc-Fe^{3+} (curve iii), the peak at 1690 cm^{-1} (C=O stretching vibration for carboxyl) in spectra of the HACC-0.20/PAAc gel (curve iv) and HACC-0.20/PAAc-Fe^{3+}-2.0 gels (curve v) shifted to 1700 cm^{-1} which can be attributed to the connection between the carboxyl groups of PAAc and the ammonium groups of HACC. In addition, a new peak was observed at 1548 cm^{-1} in the spectra of the HACC-0.20/PAAc gel (curve iv) and HACC-0.20/PAAc-Fe^{3+}-2.0 gel (curve v), which indicates also that the carboxyl groups of PAAc were linked with the ammonium groups of HACC [37, 38]. Compared with the FTIR spectra of PAAc, HACC, and the HACC-0.20/PAAc gel, the new peak at 1590 cm^{-1} in the spectra of the PAAc-Fe^{3+}-2.0 (curve ii) and HACC-0.20/PAAc-Fe^{3+}-2.0 gels (curve v) indicated the formation of metal coordination bonds.

The formation of coordination bonds between Fe^{3+} and the carboxyl group was also reflected in UV–Vis spectra (Fig. 8b). The PAAc solution, HACC solution, and HACC-0.20/PAAc hydrogel had almost no absorbance within the range of 450–650 nm. However, in the HACC/PAAc-Fe^{3+} gel, the addition of the $FeCl_3$ solution resulted in evident absorption with a shoulder peak at $\sim$ 520 nm, which indicates the formation of coordination bonds [36]. The difference in the intensities of the peaks for the HACC/PAAc-Fe^{3+}-1.4 and HACC/PAAc-Fe^{3+}-2.0 hydrogels revealed that more iron ions resulted in a higher peak absorption.

The fracture surface morphologies of the HACC-0.20/PAAc and HACC-0.20/PAAc-Fe^{3+}-2.0 gels are presented in Fig. 9. The equilibrated HACC/PAAc hydrogels had a more uniform and denser network

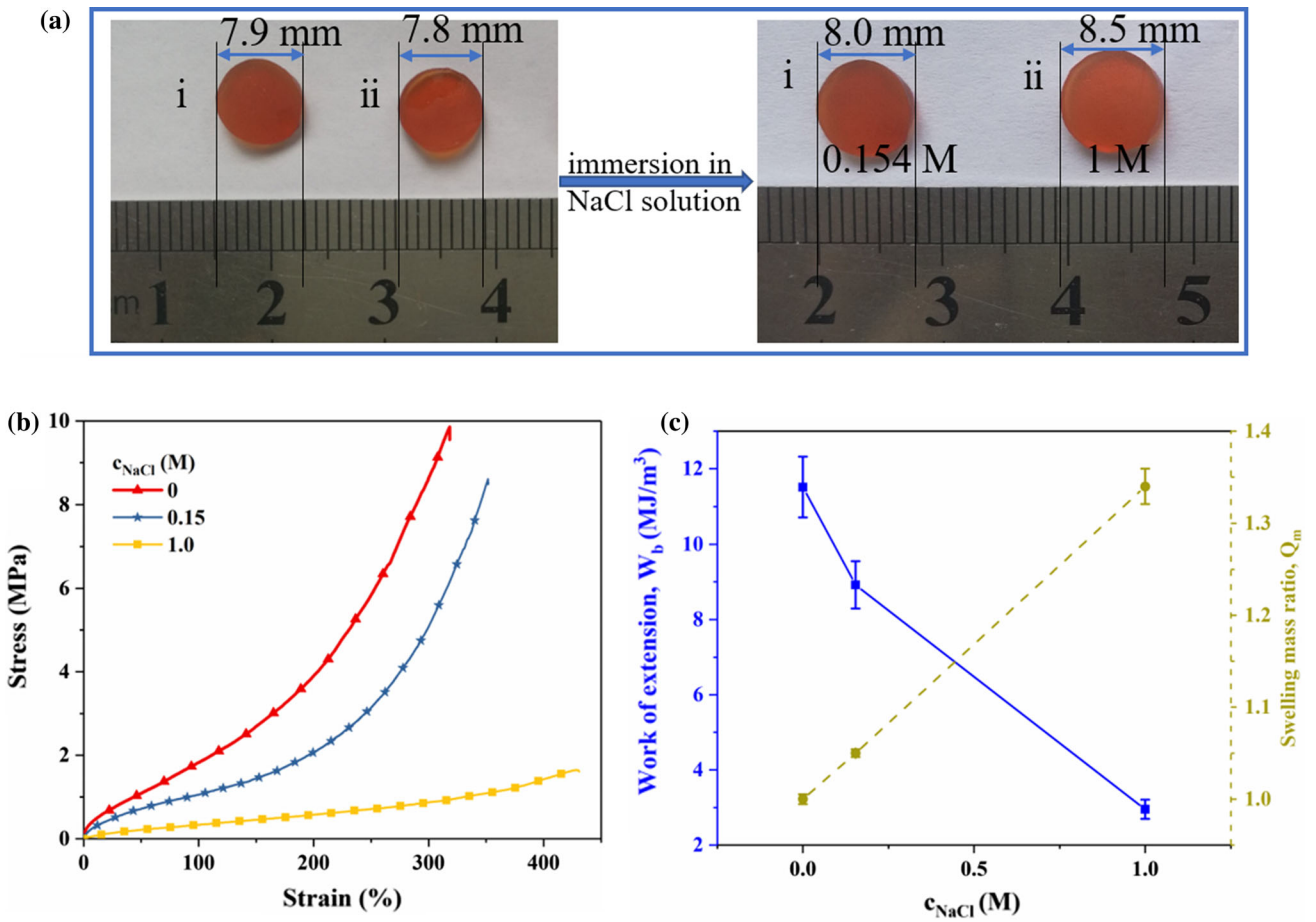

Figure 7 **a** HACC-0.20/PAAc-Fe^{3+}-2.0 hydrogels i and ii were immersed in 0. 154 M and 1 M NaCl solutions, respectively; **b** tensile behaviors of HACC-0.20/PAAc-Fe^{3+}-2.0 hydrogels after immersion in saline solutions of different concentrations c_{NaCl}; and **c** swelling ratio Q_m ($m_{swollen}/m_{original}$) and work of extension at fracture (w_b) on the concentrations of the saline solution c_{NaCl}.

structure than the as-prepared gels. The pore size was estimated by SEM images, Fig. 9a: 1.27 μm, Fig. 9b: 0.78 μm and Fig. 9c: 0.55 μm. The pore size in the equilibrated HACC/PAAc-Fe^{3+} hydrogels decreased slightly, which suggests the formation of more compact structures.

Cytotoxicity of the hydrogels

Implant materials and other biomedical applications need to be nontoxic or low toxic. In this work, the cell viability of the co-culture of the cells and hydrogels were evaluated using the CCK-8 method with 3T3 cells after incubation for 24 h and 48 h. Figure 10a verifies the cell viability of the 3T3 cells. The cell viabilities of HACC/PAAc and the HACC/PAAc-Fe^{3+} hydrogel were greater than 85%. According to ISO 10993-5-2009; when compared with the control group, if the cell survival rate is greater than 75%, the material can be identified as nontoxic. Therefore, the HACC/PAAc and HACC/PAAc-Fe^{3+} hydrogel could be identified as nontoxic, which indicates that the hydrogels are safe as biomaterials.

The 3T3 cells were seeded on a hydrogel surface, cell-adhered, and then well spread over the hydrogel surface within 24 h. As shown in Fig. 10b, c, a significant number of 3T3 cells were adhered and well spread over the surfaces of the HACC/PAAc and HACC/PAAc-Fe^{3+} hydrogels, which indicates the hydrogels did not release toxic substances. The adhesion and growth on the hydrogel surface further proved that the hydrogels are cytocompatible and can be used as biomaterials.

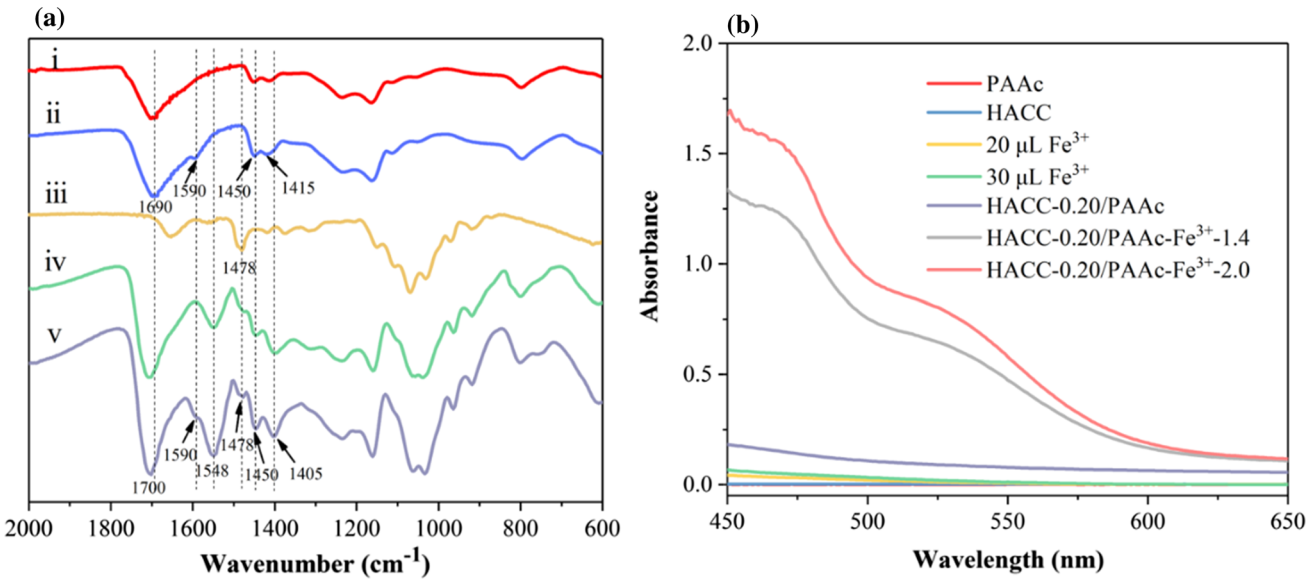

Figure 8 **a** ATR-FTIR spectra displaying the essential peaks of i pure PAAc, ii PAAc-Fe^{3+}-2.0 gel, iii pure HACC, iv HACC-0.20/PAAc gel, v HACC-0.20/PAAc-Fe^{3+}-2.0 gel and **b** UV–Vis spectra of PAAc solution (1 mg mL^{-1}) and HACC solution (1 mg mL^{-1}): 3 mL of water after addition of 20 μL or 30 μL of 0.1 M Fe^{3+} solution, HACC-0.20/PAAc gel, HACC-0.20/PAAc-Fe^{3+}-1.4 gel, and HACC-0.20/PAAc-Fe^{3+}-2.0 gel.

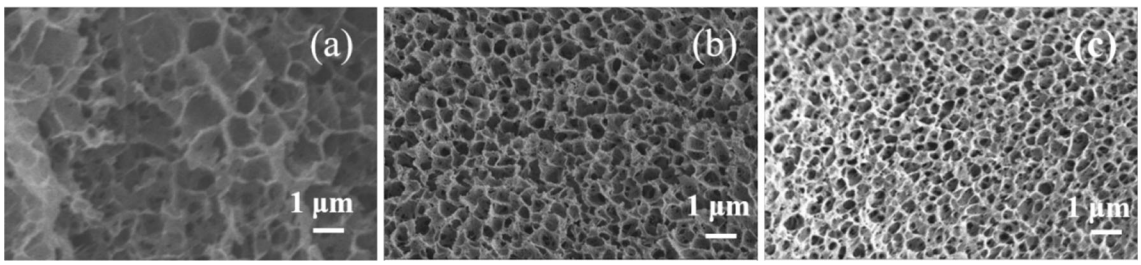

Figure 9 SEM images of microstructures of the **a** as-prepared HACC-0.20/PAAc hydrogel, **b** equilibrium state HACC-0.20/PAAc hydrogel, and **c** HACC-0.20/PAAc-Fe^{3+}-2.0 hydrogel.

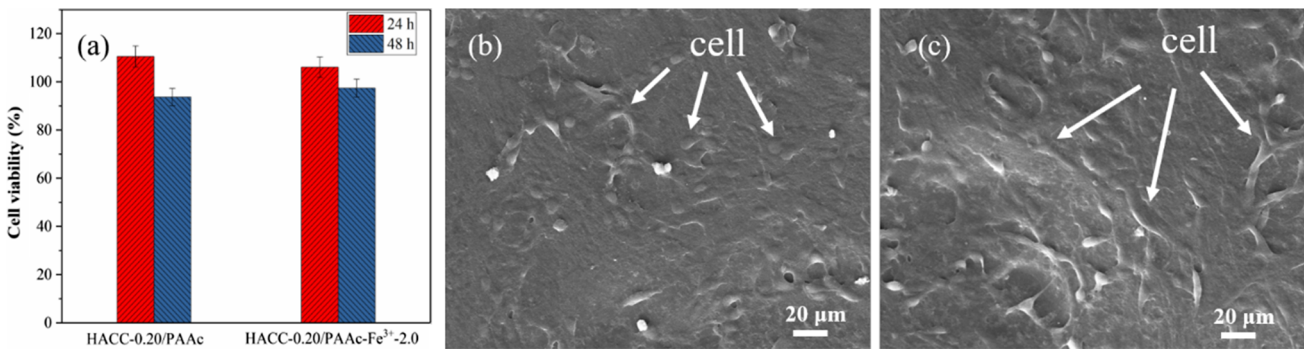

Figure 10 **a** In vitro cell viability of the HACC-0.20/PAAc and HACC-0.20/PAAc-Fe^{3+}-2.0 hydrogels. SEM images of microstructures of 3T3 cells on **b** HACC-0.20/PAAc hydrogel and **c** HACC-0.20/PAAc-Fe^{3+}-2.0 hydrogel.

Conclusion

In this study, a novel design strategy was implemented for the fabrication of a new class of dual ionically cross-linked HACC/PAAc-Fe^{3+} hydrogels using a one-pot method. The first ionic cross-link network was formed between the positively charged group of the HACC chain and the negatively charged group in the PAAC polymer chain. Moreover, the metal–ligand interactions between the Fe^{3+} and $–COO^{-}$ groups acted as the secondary ionic cross-link bonds. The dual dynamic reversible physical cross-linking improved the mechanical properties of hydrogels by effectively dissipating energy, and it resulted in excellent self-recoverability and remarkable self-healing properties. The HACC/PAAc-Fe^{3+} hydrogels did not require the addition of small molecular chemical cross-linkers, and they exhibited excellent mechanical properties. The mechanical properties of the hydrogels could be controlled by changing the concentrations of HACC and Fe^{3+}. In addition, the HACC/PAAc-Fe^{3+} hydrogels also exhibited good transparency, non-swelling, and high stabilities. Although the low water content limited the medical applications of the hydrogels, a simple, practical, one-step strategy was provided for the preparation of transparent and high-performance dual physical cross-linked hydrogels. This strategy could be applicable to other ionic hydrogels; however, further research is required.

Acknowledgements

This work was supported by the National Natural Science Foundation of China (No. 51173070), National Natural Science Foundation of Guangdong, China (No. 2016A030313097), and the Science and Technology Program of Guangzhou, China (No. 201707010264).

Compliance with ethical standards

Conflict of interest The authors declare that they have no conflict of interest.

Electronic supplementary material: The online version of this article (https://doi.org/10.1007/s10853-019-03773-5) contains supplementary material, which is available to authorized users.

References

[1] Gong JP (2010) Why are double network hydrogels so tough? Soft Matter 6:2583–2590

[2] Crompton KE, Goud JD, Bellamkonda RV, Gengenbach TR, Finkelstein DI, Horne MK, Forsythe JS (2007) Polylysine-functionalised thermoresponsive chitosan hydrogel for neural tissue engineering. Biomaterials 28:441–449

[3] Deng JN, Liang WL, Fang JY (2016) Liquid crystal droplet-embedded biopolymer hydrogel sheets for biosensor applications. ACS Appl Mater Interfaces 8:3928–3932

[4] Higa K, Kitamura N, Goto K, Kurokawa T, Gong JP, Kanaya F, Yasuda K (2017) Effects of osteochondral defect size on cartilage regeneration using a double-network hydrogel. BMC Musculoskelet Disord 18:210

[5] Lei ZY, Wang QK, Sun ST, Zhu WC, Wu PY (2017) A bioinspired mineral hydrogel as a self-healable, mechanically adaptable ionic skin for highly sensitive pressure sensing. Adv Mater 29:1700321

[6] Liu JY, Pang Y, Zhang SY et al (2017) Triggerable tough hydrogels for gastric resident dosage forms. Nat Commun 8:124

[7] Murakami K, Aoki H, Nakamura S et al (2010) Hydrogel blends of chitin/chitosan, fucoidan and alginate as healing-impaired wound dressings. Biomaterials 31:83–90

[8] Ding CX, Zhao LL, Liu FY et al (2010) Dually responsive injectable hydrogel prepared by in situ cross-linking of glycol chitosan and benzaldehyde-capped PEO-PPO-PEO. Biomacromol 11:1043–1051

[9] Chen Q, Yan XQ, Zhu L et al (2016) Improvement of mechanical strength and fatigue resistance of double network hydrogels by ionic coordination interactions. Chem Mater 28:5710–5720

[10] Gong JP, Katsuyama Y, Kurokawa T, Osada Y (2003) Double-network hydrogels with extremely high mechanical strength. Adv Mater 15:1155–1158

[11] Yang YY, Wang X, Yang F, Shen H, Wu DC (2016) A universal soaking strategy to convert composite hydrogels into extremely tough and rapidly recoverable double-network hydrogels. Adv Mater 28:7178–7184

[12] Yuan NX, Xu L, Wang HL et al (2016) Dual physically cross-linked double network hydrogels with high mechanical strength, fatigue resistance, notch-insensitivity, and self-healing properties. ACS Appl Mater Interface 8:34034–34044

[13] Haraguchi K, Takehisa T (2002) Nanocomposite hydrogels: a unique organic–inorganic network structure with extraordinary mechanical, optical, and swelling/de-swelling properties. Adv Mater 14:1120–1124

[14] Jiang HB, Wang ZF, Geng HY, Song XF, Zeng HB, Zhi CY (2017) Highly flexible and self-healable thermal interface material based on boron nitride nanosheets and a dual cross-linked hydrogel. ACS Appl Mater Inter 9:10078–10084

[15] Sakai T, Matsunaga T, Yamamoto Y et al (2008) Design and fabrication of a high-strength hydrogel with ideally homogeneous network structure from tetrahedron-like macromonomers. Macromolecules 41:5379–5384

[16] Huang T, Xu HG, Jiao KX, Zhu LP, Brown HR, Wang HL (2007) A novel hydrogel with high mechanical strength: a macromolecular microsphere composite hydrogel. Adv Mater 19:1622–1626

[17] Gu S, Duan LJ, Ren XY, Gao GH (2017) Robust, tough and anti-fatigue cationic latex composite hydrogels based on dual physically cross-linked networks. J Colloid Interface Sci 492:119–126

[18] Dai XY, Zhang YY, Gao LN, Bai T, Wang W, Cui YL, Liu WG (2015) A mechanically strong, highly stable, thermoplastic, and self-healable supramolecular polymer hydrogel. Adv Mater 27:3566–3571

[19] Li WB, An HY, Tan Y, Lu CG, Liu C, Li PC, Xu K, Wang PX (2012) Hydrophobically associated hydrogels based on acrylamide and anionic surface active monomer with high mechanical strength. Soft Matter 8:5078–5086

[20] Luo F, Sun TL, Nakajima T et al (2016) Strong and tough polyion-complex hydrogels from oppositely charged polyelectrolytes: a comparative study with polyampholyte hydrogels. Macromolecules 49:2750–2760

[21] Luo F, Sun TL, Nakajima T et al (2015) Oppositely charged polyelectrolytes form tough, self-healing, and rebuildable hydrogels. Adv Mater 27:2722–2727

[22] Sun TL, Kurokawa T, Kuroda S et al (2013) Physical hydrogels composed of polyampholytes demonstrate high toughness and viscoelasticity. Nat Mater 12:932–937

[23] Gong ZY, Zhang GP, Zeng XL, Li JH, Li G, Huang WP, Sun R, Wong CP (2016) High-strength, tough, fatigue resistant, and self-healing hydrogel based on dual physically cross-linked network. ACS Appl Mater Interfaces 8:24030–24037

[24] Feng ZB, Zuo HL, Gao WS, Ning NY, Tian M, Zhang LQ (2018) A robust, self-healable, and shape memory supramolecular hydrogel by multiple hydrogen bonding interactions. Macromol Rapid Commun 39:e1800138

[25] Wang YX, Wang ZC, Wu KL, Wu JN, Meng GH, Liu ZY, Guo XH (2017) Synthesis of cellulose-based double-network hydrogels demonstrating high strength, self-healing, and antibacterial properties. Carbohydr Polym 168:112–120

[26] Hu Y, Du ZS, Deng XL, Wang T, Yang ZH, Zhou WY, Wang CY (2016) Dual physically cross-linked hydrogels with high stretchability, toughness, and good self-recoverability. Macromolecules 49:5660–5668

[27] Cai TT, Huo SJ, Wang T, Sun WX, Tong Z (2018) Self-healable tough supramolecular hydrogels crosslinked by poly-cyclodextrin through host-guest interaction. Carbohydr Polym 193:54–61

[28] Han L, Yan LW, Wang KF et al (2017) Tough, self-healable and tissue-adhesive hydrogel with tunable multifunctionality. NPG Asia Mater 9:e372

[29] Burattini S, Colquhoun HM, Fox JD et al (2009) A self-repairing, supramolecular polymer system: healability as a consequence of donor-acceptor π–π stacking interactions. Chem Commun 44:6717–6719

[30] Wang X-H, Song F, Qian D, He Y-D, Nie W-C, Wang X-L, Wang Y-Z (2018) Strong and tough fully physically cross-linked double network hydrogels with tunable mechanics and high self-healing performance. Chem Eng J 349:588–594

[31] He QY, Huang Y, Wang SY (2018) Hofmeister effect-assisted one step fabrication of ductile and strong gelatin hydrogels. Adv Funct Mater 28:1705069

[32] Ren Y, Lou RY, Liu XC et al (2016) A self-healing hydrogel formation strategy via exploiting endothermic interactions between polyelectrolytes. Chem Commun 52:6273–6276

[33] Zhao YR, Li MN, Liu BC et al (2018) Ultra-tough injectable cytocompatible hydrogel for 3D cell culture and cartilage repair. J Mater Chem B 6:1351–1358

[34] Yuan NX, Xu L, Xu B, Zhao JH, Rong JH (2018) Chitosan derivative-based self-healable hydrogels with enhanced mechanical properties by high-density dynamic ionic interactions. Carbohydr Polym 193:259–267

[35] Duan JJ, Liang XC, Cao Y, Wang S, Zhang LN (2015) High strength chitosan hydrogels with biocompatibility via new avenue based on constructing nanofibrous architecture. Macromolecules 48:2706–2714

[36] Zheng SY, Ding HY, Qian J, Yin J, Wu ZL, Song YH, Zheng Q (2016) Metal-coordination complexes mediated physical hydrogels with high toughness, stick-slip tearing behavior, and good processability. Macromolecules 49:9637–9646

[37] Song YB, Zhou JP, Li Q, Guo Y, Zhang LN (2009) Preparation and characterization of novel quaternized cellulose nanoparticles as protein carriers. Macromol Biosci 9:857–863

[38] You J, Xie SY, Cao JF, Ge H, Xu M, Zhang LN, Zhou JP (2016) Quaternized chitosan/poly(acrylic acid) polyelectrolyte complex hydrogels with tough, self-recovery, and tunable mechanical properties. Macromolecules 49:1049–1059